Microwave Absorption Behavior of Core−Shell Structured Poly (3,4-Ethylenedioxy Thiophene)−Barium Ferrite Nanocomposites

Anil Ohlan,[†,‡] Kuldeep Singh,[†] Amita Chandra,[‡] and Sundeep K. Dhawan*[,†]

Polymeric and Soft Materials Section, National Physical Laboratory (CSIR), Dr. K. S. Krishnan Road, New Delhi 110012, India and Department of Physics and Astrophysics, University of Delhi, Delhi 110 007, India

ABSTRACT The present paper reports the complex permittivity, permeability, and microwave absorption properties of core shell type poly (3,4-ethylenedioxy thiophene) (PEDOT) nanocomposite with barium ferrite, synthesized by in situ emulsion polymerization, in the 12.4−18 GHz frequency range. High-resolution transmission electron microscopy (HRTEM) studies reveal the formation of core−shell type morphology with ferrite particles (60−80 nm) as the center while the polymer (PEDOT) formulates the outer shell of the composite. The presence of barium ferrite nanoparticles in the polymer matrix includes the magnetic losses, which mainly arise from the magnetic hysteresis, domain−wall displacement, and eddy current loss. The higher dielectric ($\varepsilon'' = 23.5$) and magnetic loss ($\mu'' = 0.22$) contributes to the microwave absorption value of 22.5 dB (>99% attenuation) and are found to increase with the amount of ferrite constituents. The polymer was further characterized through Fourier transform infrared spectroscopy (FTIR), energy dispersive X-ray spectroscopy (EDS), and X-ray diffraction (XRD).

KEYWORDS: permittivity • permeability • nanocomposites • microwave absorption • conjugated polymers

INTRODUCTION

Polymer and polymer-based composites with electroconductive properties have found numerous uses in technological applications like energy storage (1), antistatic packaging (2, 3), electro-optical devices (4, 5), welding of plastics (6), and electromagnetic shielding (7−10). With the rapid development of the electronics industry, the dominant frequency range of communication devices has shifted toward a higher range in order to enhance the data transfer rates. As a result, the demand for the microwave absorbers and electromagnetic shields in this frequency range is increasing, to solve the electromagnetic interference (EMI) problems. The microwave-absorption properties are determined by the relative permeability, permittivity, electromagnetic impedance matching, and the microstructure of the absorber. Among the electromagnetic wave absorbers, spinel-type ferrites (11−13), metallic magnetic materials (14−19), and carbon nanotube (CNT) composites (20−24) have been extensively studied. However, the spinel-type ferrites show Snoek's limit (25) due to which magnetic losses decreases drastically at gigahertz frequency. Metallic magnetic materials (26, 27) show high permeability, but they have to be insulated, to prevent an eddy current due to a drop in the complex permeability (μ_r) in the gigahertz range. Yang et al. (28) reported a CNT polystyrene foam structure composite with EMI shielding effectiveness (SE) of 19 dB, and Che et al. (29) reported the synthesis of CNT encapsulated with Fe nanoparticles showing good absorption behavior but the complex synthesis of CNT filled with magnetic nanoparticles is not favorable for practical applications. The hexagonal-type ferrites are suitable as a radar absorbing materials (RAM) due to a large value of permeability, high value of magnetization, and planar anisotropic behavior, as well as good dielectric properties at microwave frequencies. However, for high attenuation (30−33), thick samples are required.

Among the candidates for electromagnetic wave absorbers, conducting polymer−ferrite composites may be potential candidates for microwave absorption materials at high frequencies over the gigahertz range due to their high dielectric and magnetic losses. Different strategies have been employed for the preparation of these type polymer composites. Typically, chemical polymerization of monomer in the presence of inorganic dopant like HCl, H_2SO_4, is carried out using oxidants like ammonium peroxydisulphate and $FeCl_3$. When organic dopants with surfactant functionalities are used, emulsions or micelles can be formed leading to microtubes, fibers, or rodlike structures. However, if nanostructures with diameters of 100 nm are desired, then complex dopants with bulky side groups are needed, such as sulfonated naphthalene derivatives and camphor sulfonic acid. Recently, micellar solutions of sodium dodecyl sulfate (SDS) and sodium dodecyl benzene sulfonate (SDBS) were employed to produce colloidal polymeric particles dispersible in water. Previous reports mainly focused on the effect of monomer and surfactant concentration on composition, morphology, crystalline nature, and conductivity of polymer. Earlier, studies have been done on the development of

* Corresponding author. E-mail: skdhawan@mail.nplindia.ernet.in. Phone: +91-11-45609401. Fax: +91-11-25726938.
Received for review December 15, 2009 and accepted February 17, 2010
† National Physical Laboratory (CSIR).
‡ University of Delhi.
DOI: 10.1021/am900893d

Scheme 1. Schematic Representation of (a) Polymerization of EDOT Containing the Barium Ferrite Nanoparticles Using APS as Oxidant and (b) the Interaction of the Microwave with the Polymer Composite Resulting in Its Attenuation Due to the Scattering with the Nanoparticles

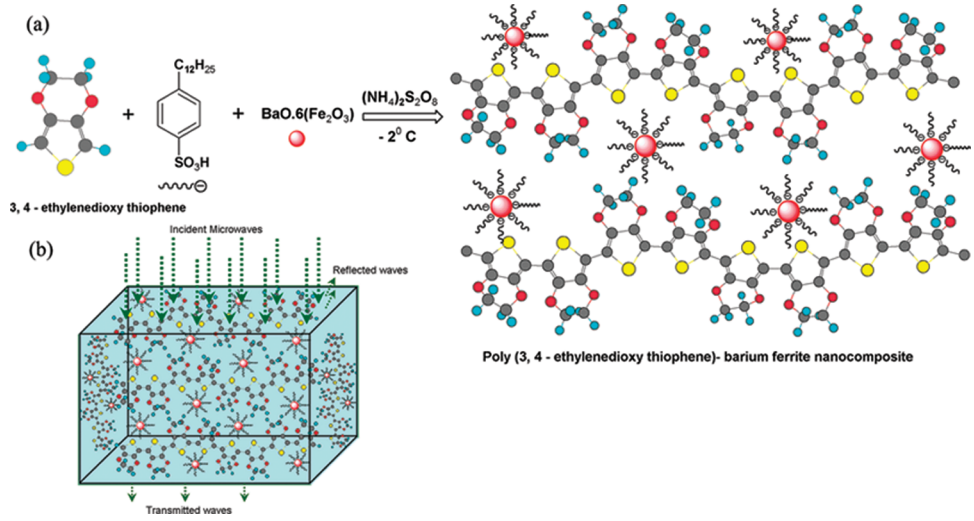

composites having both conducting and ferromagnetic properties by the incorporation of ferrite particles such as Fe_3O_4, manganese−zinc ferrite particles (34−37).

In the present work, we explore that the synthesis of conducting poly (3,4-ethylenedioxy thiophene) (PEDOT) composite with bulky dodecyl benzene sulfonic acid (DBSA) with the dual role of surfactant and dopant, leading to the formation of a core−shell like structure. This core−shell like structure contributes toward higher microwave absorption (>99% attenuation). However, to our knowledge, there are no detailed reports on the upshot of core shell structured composite on the microwave absorption properties. A systematic study in this direction is particularly important because the presence of magnetic core having conducting shell can significantly change the absorption of electromagnetic radiation to great extent. Here, we report the complex permittivity, permeability and microwave absorption properties of poly (3,4-ethylenedioxy thiophene) (PEDOT) nanocomposite with barium ferrite (60−80 nm). Barium ferrite is selected due to its high resistivity and high magnetic losses whereas PEDOT is chosen because of its moderate conductivity ($\sim 10^{-2}$ S/cm) and dielectric properties so that both contribute toward higher microwave absorption (>99% attenuation). The effect of ferrite constituent on complex permittivity, permeability, and the microwave absorption properties of the PEDOT nanocomposite have been investigated and compared with the pristine PEDOT−DBSA.

EXPERIMENTAL SECTION

The synthesis of barium ferrite (BaF) has been carried out via precursor route (38) by dissolving 1:12:13 molar ratio of barium nitrate, ferric nitrate, and citric acid, respectively, in distilled water. The ferrite particles have further been grinded for 6 h using a Retsch "PM-400" planetary-ball mill in tungsten carbide jars. The resulting ferrite nanoparticles (60−80 nm) have been homogenized in 0.3 M aqueous solution of dodecyl benzene sulfonic acid (DBSA) to form a whitish brown emulsion solution. To the above solution, 0.1 M of EDOT (3,4-ethylene dioxy thiophene) has been added which has again been homogenized for 2 to 3 h to form micelles of EDOT with barium ferrite. The micelles so formed have been polymerized at −2 °C by emulsion polymerization using APS ($(NH_4)_2S_2O_8$) (0.1 M) as oxidant. The product so obtained has been demulsified by treating it with an equal amount of isopropyl alcohol. The precipitate, thus, obtained has been filtered, washed, and dried at 60−65 °C. The effect of the concentration of BaF nanoparticles on the microwave absorption properties of the resulting PEDOT−BaF nanocomposites has been studied by modulating weight ratios of EDOT monomer to BaF nanoparticles [EDOT/BaF] at 2:1 (PEDOT−BaF21), 1:1 (PEDOT−BaF11), and 1:2 (PEDOT−BaF12), respectively. In addition, polymer without ferrite particles (PEDOT−DBSA) has been synthesized for comparative study.

Characterization. The particle size and the morphology of barium ferrite and polymer composites have been examined using a high-resolution transmission electron microscopy (HR-TEM, Tecnai G^2 F30 S-Twin) instrument operating at an accelerating voltage of 300 kV, having a point resolution of 0.2 nm and a lattice resolution of 0.14 nm. The presence of barium ferrite in the polymer composite has been confirmed by X-ray diffraction (XRD) studies carried out on D8 Advance X-ray diffractometer (Bruker) using Cu Kα radiation (λ= 1.540598 Å) in scattering range (2θ) of 10−70° with a scan rate of 0.02°/sec and slit width of 0.1 mm. Electromagnetic shielding and dielectric measurements have been carried out on an Agilent E8362B Vector network analyzer in the frequency range of 12.4−18 GHz (Ku-band). Powder samples have been compressed in rectangular pellets (15.8 × 7.9 mm^2) and inserted in a copper sample holder, which has been connected between the waveguide flanges of network analyzer. Fourier transform infrared spectroscopy (FTIR) spectra were recorded on Nicolet 5700 in transmission mode, wavenumber range 400−4000 cm^{-1}. The spectroscopic grade KBr discs has been used for collecting the spectra with a resolution of 4 cm^{-1} performing 32 scans.

RESULTS AND DISCUSSION

The formation of PEDOT−barium ferrite composite has been carried out using emulsion polymerization (oil in water type) in which the droplet of EDOT (oil) emulsified with surfactant DBSA containing ferrite particles, in a continuous phase of water. A large amount of surfactant lead to the formation of micelle which in aqueous solution forms a

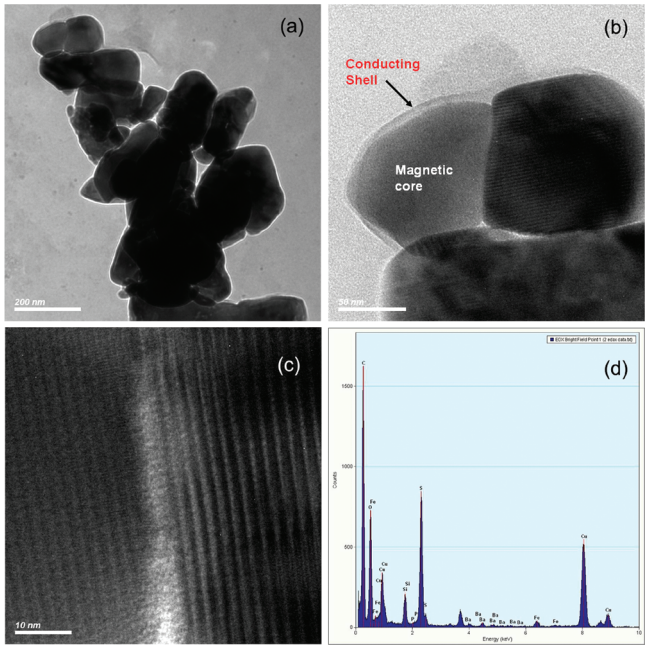

FIGURE 1. Low magnification HRTEM image of PEDOT−BaF12 (a) and PEDOT−BaF11 (b) nanocomposites, showing the core−shell morphology with barium ferrite as the core and PEDOT forms the capping of nanoparticles. (c) High magnification HRTEM image of PEDOT−BaF12 showing the (114) oriented lattice planes of barium ferrite and (d) energy dispersive X-ray spectroscopy pattern (EDS) of PEDOT−BaF12 showing the approximate percentage of the elements present in the nanocomposite.

roughly spherical or globular aggregate with the hydrophilic "head" regions in contact with surrounding solvent, sequestering the hydrophobic tail regions in the micelle center. When monomer EDOT is added to the micellar solution containing nanoparticles, it diffuses through water to micelles. The addition of oxidant APS to the solution leads to the oxidative polymerization where EDOT is oxidized and forms EDOT radical cations, which subsequently combine with another unit to form a neutral dimer. The further oxidation of this dimer leads to the formation of a trimer and finally to a polymer containing nanoparticles of barium ferrite embedded in between the polymer chains as shown in Scheme 1a.

HRTEM and XRD Analysis. Figure 1 demonstrates the high-resolution transmission electron microscopy (HRTEM) images and energy dispersive X-ray spectroscopy (EDS) pattern of PEDOT−BaF nanocomposites. HRTEM images of PEDOT−BaF11 (Figure 1a) and PEDOT−BaF12 (Figure 1b) clearly indicate that the in situ emulsion process leads to the formation of core−shell type morphology with ferrite particles as the center while the polymer (PEDOT) forms the covering. The shell of the particle gives an impression of an amorphous layer, as no fringes have been observed at the shell. The lattice plane spacing of the core ferrite particles is about 0.26 nm, which corresponds to the (114) plane of a barium ferrite phase (Figure 1c). The elemental analysis of the composite has been performed using energy dispersive X-ray pattern as shown in Figure 1d. The peak of sulfur is due to dopant DBSA while Cu and Si are the impressions of copper grid and the silicon detector.

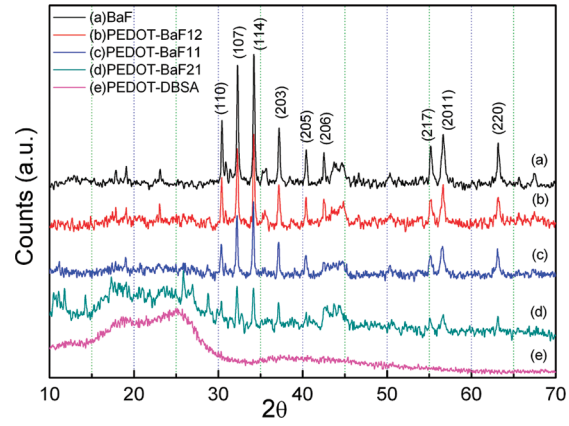

FIGURE 2. X-ray diffraction patterns of (a) BaF, (b) PEDOT−BaF12, (c) PEDOT−BaF11, (d) PEDOT−BaF21, and (e) PEDOT−DBSA. Plots b, c, and d confirm the presence of barium ferrite in the polymer composites.

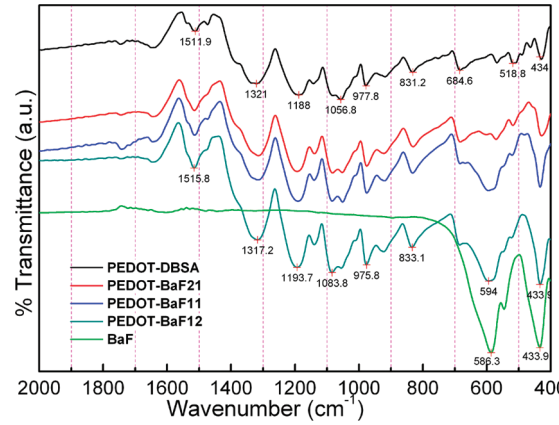

FIGURE 3. Comparison of FTIR spectra of BaF, PEDOT−DBSA, and PEDOT−BaF composites, having different ferrite ratios, showing the absence of chemical interaction between ferrite particles and PEDOT.

X-ray diffraction (XRD) patterns of the composites also confirm the presence of barium ferrite particles (39) in PEDOT matrix (Figure 2). In XRD patterns, PEDOT−DBSA shows two broad peaks at $2\theta = 19°$ and 25°, which reveals its amorphous nature. With the addition of ferrite particle, the peaks of barium ferrite start appearing. In PEDOT−BaF21, due to the low concentration of ferrite particles, the intensity of ferrite peaks is small and only the intense peaks were noticeably observed. As the loading of the ferrite particles increase, in PEDOT−BaF11and PEDOT−BaF12, all the peaks of crystalline barium ferrite were clearly revealed, which indicates the increase of crystalline barium ferrite phase in the composite. The presence of conducting shell encapsulating the magnetic and dielectric nanoparticles is helpful for the proper impedance matching, which is necessary for enhancing the absorption of the electromagnetic wave.

Fourier-Transform Infrared Spectroscopy (FTIR) Investigations. Figure 3 demonstrates the Fourier-transform infrared spectroscopy (FTIR) spectra of barium ferrite, PEDOT−DBSA, and PEDOT−BaF composites. The vibrational bands at around 1321 cm^{-1} and 1512 cm^{-1} are due to C−C or C═C stretching of the quinoid structure of the thiophene ring and due to ring stretching of the thiophene

ring, respectively. Vibrational bands at 1188 cm^{-1}, 1145 cm^{-1}, and 1056 cm^{-1} arise due to C−O−C bond stretching in the ethylene dioxy group. C−S bond in the thiophene ring are also seen at 978, 831, and 684 cm^{-1}. The peak at 1330 cm^{-1} has been reported to be the main characteristic peak of PEDOT (40). The FTIR spectra of barium ferrite shows characteristic peaks at 586, 546, and 434 cm^{-1} which are due Fe−O bond stretching. The presence of a band at 594 cm^{-1} in the composite clearly shows the presence of barium ferrite in the composite which was absent in PEDOT−DBSA. The shift in the main peaks of PEDOT has been observed by the incorporation of ferrite particles, which confirms that some interaction of ferrite nanoparticles takes place with polymer chains. However, the intensity of the Fe−O stretching vibration modes is affected by the [EDOT]/[BaF] ratio. For instance, the band of Fe−O stretching vibration modes in the composites at a higher [EDOT]/[BaF] ratio is weaker because the hexagonal barium ferrite nanoparticles are completely enwrapped by the polymer (PEDOT). Especially, there is no new band in FTIR spectra of the composites indicating that there is no chemical reaction between barium ferrite and PEDOT and only a small interaction takes place due to the capping to ferrite particles in the polymer. Most prominent change was observed in the vibrational bands at 1512 cm^{-1} (C═C stretching of quinoid structure) which has a split at 1475 cm^{-1}. In case of PEDOT−BaF composite, the peak area of this band increases while the intensity of the splitting decreases with the ferrite content. The characteristic peaks at 1325 cm^{-1}, assigned to C−C, shifts to 1313 cm^{-1}, and an increase in the peak area and intensity is observed, which further increases with the barium ferrite loading in the polymer. In addition, the peak intensity of the C−S band assigned at 978, 831, and 684 cm^{-1} increases with the increase of ferrite content. Moreover, in PEDOT−DBSA, the band observed at 1088 cm^{-1} (C−O−C stretching) has a split at 1057 cm^{-1}. The addition of barium ferrite resolved this splitting into 1082 and 1051 cm^{-1}, and the intensity of the 1051 cm^{-1} band increases with the increase of ferrite content. This increase in peak area and intensity is because the addition of barium ferrite leads to increases in the polarization that ultimately increases the dipole interaction. This is also in harmony with the microwave absorption property, which depends on strong polarization that consequently leads to the improved values.

Microwave Absorption Measurements. The EMI shielding effectiveness (SE) of a material can be expressed as

$$SE(dB) = -10 \log \frac{P_t}{P_0} = SE_R + SE_A + SE_M \qquad (1)$$

where P_t and P_0 are the transmitted and incident electromagnetic power, respectively. The terms in eq 1 can be described as (41) $SE_R = -10 \log (1 - R)$ and $SE_A = -10 \log [T/(1 - R)]$. SE_R and SE_A are the shielding effectiveness due to reflection and absorption, respectively (Scheme 1b). SE_M is multiple reflection effectiveness inside the material, which can be negligible when SE >10 *dB*. Figure 4 shows the variation of the shielding effectiveness with frequency for the different ratios of the [EDOT]/[BaF]. As compared to the lower SE of PEDOT−DBSA, the SE of the composite increases with the ferrite content exhibiting excellent frequency stability in the measured frequency range. The contribution to the SE values mainly comes from the absorption rather than reflection in the case of PEDOT−BaF composites. PEDOT−BaF12 has the higher SE_A of 22.4 dB with nominal SE_R of 2 dB as compared to SE_A value of 8 dB and comparable reflection SE_R of 6 dB for the PEDOT−DBSA. The increase in the absorption part with the addition of ferrite particles may be attributed to the higher dielectric and magnetic losses observed in the polymer composites while in the case of PEDOT−DBSA, only dielectric losses contributed to the SE_A values. The dependence of SE on complex permittivity and permeability can be expressed as (42)

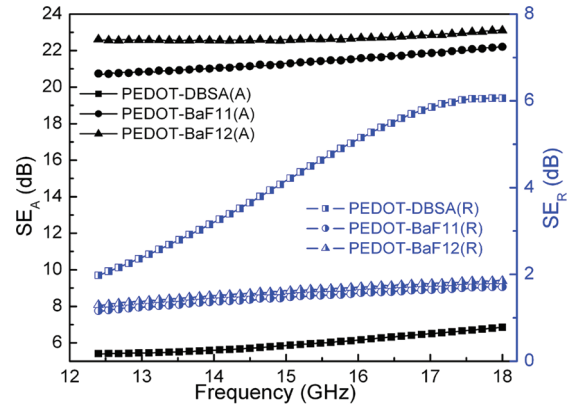

FIGURE 4. Dependence of shielding effectiveness (SE_A and SE_R) as a function of frequency showing the effect of barium ferrite concentration on the SE_A value of the nanocomposites.

$$SE_A(dB) = 20\frac{d}{\delta} \log e = 20d\sqrt{\frac{\mu_r \omega \sigma_{AC}}{2}} \cdot \log e \qquad (2)$$

$$SE_R(dB) = 10 \log\left(\frac{\sigma_{AC}}{16\omega\mu_r\varepsilon_0}\right) \qquad (3)$$

where, d is the thickness of the shield, μ_r is the magnetic permeability, δ is the skin depth, $\sigma_{AC} = \omega\varepsilon_0\varepsilon''$ is the frequency dependent conductivity (43); ε'' is the imaginary part of permittivity (dielectric loss factor), ω is the angular frequency ($\omega = 2\pi f$), and ε_0 is the permittivity of the free space. From eqs 2 and 3, it is observed that with the increase in frequency, the SE_A values increases while the contribution of the reflection decreases. Dependence of SE_A and SE_R on conductivity and permeability revel that the material having higher conductivity and magnetic permeability can achieve better absorption properties.

Complex Permittivity Results. Complex permittivity and the permeability of PEDOT−BaF composites have been calculated using scattering parameters (S_{11} and S_{21}) based on the theoretical calculations given in the Nicholson, Ross, and Weir method (44, 45). The real part

(ε') is mainly associated with the amount of polarization occurring in the material and the imaginary part (ε'') is related with the dissipation of energy. The dielectric performance of the material depends on ionic, electronic, orientational, and space charge polarization. The contribution to the space charge polarization appears due to the heterogeneity of the material. The presence of insulating barium ferrite in the conducting matrix results in the formation of more interface and a heterogeneous system due to some space charge accumulating at the interface that contributes toward the higher microwave absorption in the composites. The contribution to the orientational polarization is due to the presence of bound charges (dipoles). In conjugated polymers, two types of charged species are present: one polaron/bipolaron system that is mobile and free to move along the chain and others are bound charges (dipoles) which have only restricted mobility and account for strong polarization in the system (46). When the frequency of the applied field is increased, the dipoles present in the system cannot reorient themselves fast enough to respond to applied electric field, and as a result, dielectric constant decreases. Due to the difference in the dielectric constant and conductivity of barium ferrite and PEDOT, some charge carriers present in PEDOT were trapped, and as a result, space charge is developed at the interface of the ferrite particles and the polymer. This also leads to the generation of some space charge at the heterogeneous interface leading to field distortion. As the frequency of applied electric field is reduced, the contribution of ionic conduction toward the total loss becomes prominent. With the increase in frequency, the tendency for the interfacial polarization is expected to be decreased resulting in a decrease in polarizability and loss factor. Therefore, with the increase in frequency, ε' and ε'' decreases. From Figure 5a,b, it is observed that in PEDOT−DBSA both the real and imaginary part of the permittivity remains constant in the measured frequency range. While in the case of PEDOT−BaF composites, incorporation of insulating barium ferrite in the conducting matrix shows higher values of ε' and ε'' as compared to PEDOT−DBSA. The higher values of ε' and ε'' arise due to the difference in the relative dielectric constant of barium ferrite and the PEDOT, which results in the accumulation of more space charge, and strong orientational polarization that consequently leads to the improved values of microwave absorption.

Complex Permeability Studies. Figure 6 shows the variation in the real (μ') and imaginary (μ'') parts of permeability with frequency for the PEDOT−BaF composites with different [EDOT]/[BaF] ratios. The real part of the permeability remains constant with a little fluctuation in the measured frequency range whereas the magnetic loss part slightly decreases with the frequency. Higher values of μ'' have been observed for PEDOT−BaF12 as compared to PEDOT−BaF11, which confirms the existence of greater magnetic losses in the PEDOT−BaF12 nanocomposite. The magnetic loss is expressed by the imaginary part of complex permeability and mainly occurs because of magnetic hysteresis and domain−wall displacement in the material. The permeability (47) for the hexagonal ferrites having the *c*-axis as the preferred direction of magnetization is defined as

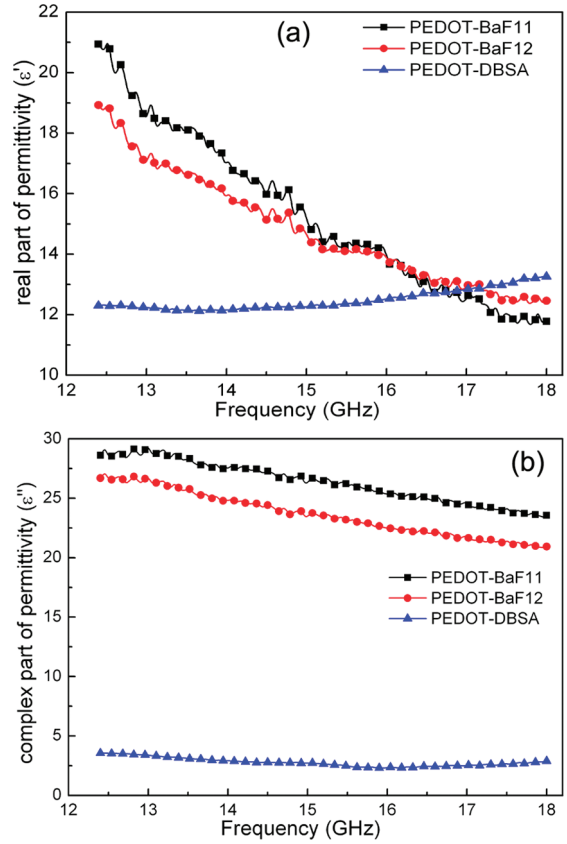

FIGURE 5. Behavior of (a) real and (b) imaginary part of complex permittivity PEDOT−BaF composites as a function of frequency.

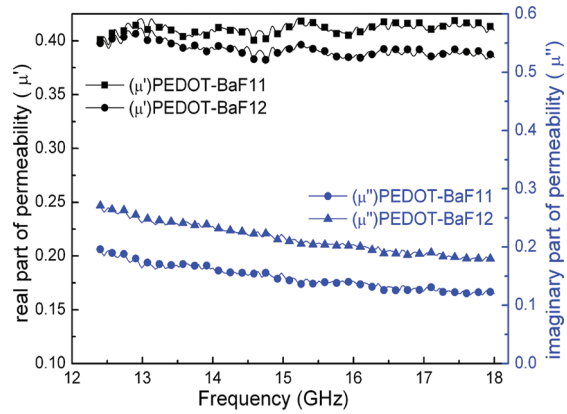

FIGURE 6. Variation of real and imaginary part of magnetic permeability of PEDOT−BaF composites as a function of frequency.

$$\frac{(\mu - 1)}{4\pi} = \left(\frac{2}{3}\right)\frac{M_S}{H_A} \qquad (4)$$

where M_S is the saturation magnetization and H_A is the anisotropy field. As the frequency increases, μ remains equal to its static (dc) value up to a critical frequency and then decreases with the further increase in frequency. Whereas, the imaginary part of permeability (μ'') starts increasing near the critical frequency and has a maxima at the resonance

frequency, which demonstrates the maximum power loss. The larger the static value of μ, the lower is the frequency at which this decrease occurs as given by Snoek's law (25). The frequency of this precession depends on how strongly the magnetization is bound to the easy axis. The stronger the coupling, higher is the natural frequency of precession. The strength of this coupling depends on the value of the magneto-crystalline anisotropy K or the anisotropy field H_A, which is proportional to H_A (47). In barium ferrite, due to the large anisotropy field, the coupling of the magnetic dipole is strong. When the frequency of the applied field increases, the magnetic dipole tries to rotate with the frequency but at higher frequency due to strong anisotropy, the induced magnetization (B) lags behind the applied field (H) which results in magnetic losses. The larger is the anisotropy, higher is the difference in B and H and more are the magnetic losses occurring in the material (48). In magnetic nanoparticles, the rotation of domains becomes difficult due to the effective anisotropy (magneto-crystalline anisotropy and shape anisotropy). The effective anisotropy coefficient can be enhanced significantly with decreasing particle size, due to the surface effect and microstructure defects (49, 50). Therefore, the increase in barium ferrite content in the polymer matrix leads to higher magnetic loss, which in turn enhances absorption of the microwaves. The dielectric and magnetic loss in the whole frequency range proves the balanced property of EM matching in the composite, suggesting that the enhanced microwave absorption properties unambiguously result from the cooperative effect of PEDOT shell and ferrite cores.

CONCLUSIONS

In conclusion, PEDOT−BaF nanocomposite demonstrates strong microwave absorption properties in 12.4−18 GHz with SE_A value of 22.5 dB at 15 GHz with minimal reflection loss of 2 dB. The high absorption properties mainly result from the high dielectric and magnetic losses in the composites and depend on the concentration of barium ferrite in the polymer composite. The in situ emulsion polymerization, which results in core−shell type morphology, enhances the interfacial polarization and the effective anisotropic energy of the composite, which contributes to the higher microwave absorption. As a result, nanocomposites with dielectric shells and ferrite cores are also promising as new types of microwave absorptive materials with usability in a wide frequency range maintaining strong absorption.

Acknowledgment. The authors wish to thank the Director, N.P.L., for his keen interest in the work. The authors also thank Dr. Rashmi and Dr. Renu Pasricha for recording XRD pattern and HRTEM measurements of the samples. A.O. and K.S. are thankful to CSIR for providing the necessary fellowship.

REFERENCES AND NOTES

(1) Park, K. S.; Schougaard, S. B; Goodenough, J. B. *Adv. Mater.* **2007**, *19*, 848–851.
(2) Virtanen, E.; Laakso, J.; Ruohonon, H.; Vakiparta, K.; Jarvinen, H.; Jussila, M.; Passiniemi, P.; Osterhanm, J. E. *Synth. Met.* **1997**, *84*, 113–114.
(3) Soto-Oviedo, M. A.; Araujo, O. A.; Faez, R.; Rezende, M. C.; De Paoli, M. A. *Synth. Met.* **2006**, *156*, 1249–1255.
(4) Cao, Y.; Treacy, G. M.; Smith, P.; Hegger, A. J. *Synth. Met.* **1993**, *55*, 3526–3531.
(5) Chiang, C. K.; Gau, S. C.; Fincher, C. R.; Park, Y. W.; MacDiarmid, A. G.; Heeger, A. *J. Appl. Phys. Lett.* **1978**, *33*, 18.
(6) Wu, C. Y.; Benatar, A. *Polym. Eng. Sci.* **1997**, *37*, 738–743.
(7) Ohlan, A.; Singh, K.; Chandra, A.; Dhawan, S. K. *J. Appl. Polym. Sci.* **2008**, *108*, 2218–2225.
(8) Phang, S. W.; Hino, T.; Abdullah, M. H.; Kuramoto, N. *Mater. Chem. Phys.* **2007**, *104*, 327–335.
(9) Dhawan, S. K.; Singh, N.; Venkatachalam, S. *Synth. Met.* **2002**, *129*, 261–267.
(10) Chandrasekhar, P.; Naishadham, K. *Synth. Met.* **1999**, *105*, 115–120.
(11) Yoshida, S.; Sato, M.; Sugawara, E.; Shimada, Y. *J. Appl. Phys.* **1999**, *85*, 4636.
(12) Ghasemi, A.; Saatchi, A.; Salehi, M.; Hossienpour, A.; Morisako, A.; Liu, X. *Phys. Status Solidi A* **2006**, *203*, 358–365.
(13) Xie, J. L.; Han, M.; Chen, L.; Kuang, R.; Deng, L. *J. Magn. Magn. Mater.* **2007**, *314*, 37–42.
(14) Lu, B.; Dong, X. L.; Huang, H.; Zhang, X. F.; Zhu, X. G.; Lei, J. P; Sun, J. P. *J. Magn. Magn. Mater.* **2008**, *320*, 1106–1111.
(15) Liu, J. R.; Itoh, M.; Horikawa, T.; Machida, K.; Sugimoto, S.; Maeda, T. *J. Appl. Phys.* **2005**, *98*, 054305.
(16) Liu, J. R.; Itoh, M.; Machida, K. *Appl. Phys. Lett.* **2003**, *83*, 4017.
(17) Sugimoto, S.; Maeda, T.; Book, D.; Kagotani, T.; Inomata, K.; Homma, M.; Ota, H.; Houjou, Y.; Sato, R. *J. Alloys Compd.* **2002**, *330*, 301–306.
(18) Liu, X. G.; Geng, D. Y.; Meng, H.; Shang, P. J.; Zhang, Z. D. *Appl. Phys. Lett.* **2008**, *92*, 173117.
(19) Li, B. W.; Shen, Y.; Yue, Z. X.; Nan, C. W. *Appl. Phys. Lett.* **2006**, *89*, 132504.
(20) Che, R. C.; Zhi, C. Y.; Liang, C. Y.; Zhou, X. G. *Appl. Phys. Lett.* **2006**, *88*, 033105.
(21) Watts, P. C. P.; Hsu, W. K.; Barnes, A.; Chambers, B. *Adv. Mater.* **2003**, *15*, 600–603.
(22) Makeiff, D. A.; Huber, T. *Synth. Met.* **2006**, *156*, 497–505.
(23) Wadhawan, A.; Garrett, D.; Perez, J. M. *Appl. Phys. Lett.* **2003**, *83*, 29.
(24) Xu, H.; Anlage, S. M.; Hu, L.; Grunera, G. *Appl. Phys. Lett.* **2007**, *90*, 183119.
(25) Snoek, J. L. *Physica (Amsterdam)* **1948**, *14*, 207–217.
(26) Zhang, X. F.; Dong, X. L.; Huang, H.; Lv, B.; Lei, J. P.; Choi, C. J. *J. Phys. D: Appl. Phys.* **2007**, *40*, 5383–5387.
(27) Liu, X. G.; Ou, Z. Q.; Geng, D. Y.; Han, Z.; Xie, Z. G.; Zhang, Z. D. *J. Phys. D: Appl. Phys.* **2009**, *421*, 55004.
(28) Yang, Y. L.; Gupta, M. C.; Dudley, K. L.; Lawrence, R. W. *Nano Lett.* **2005**, *5*, 2131–2134.
(29) Che, R. C.; Peng, L. M.; Duan, X. F.; Chen, Q.; Liang, X. L. *Adv. Mater.* **2004**, *16*, 401–405.
(30) Abbas, S. M.; Chatterjee, R.; Dixit, A. K.; Kumar, A. V. R.; Goel, T. C. *J. Appl. Phys.* **2007**, *101*, 074105.
(31) Nie, Y.; He, H. H.; Feng, Z. K.; Zhang, X. C.; Cheng, X. M. *J. Magn. Magn. Mater.* **2006**, *303*, e423–e427.
(32) Oikonomou, A.; Giannakopoulou, T.; Litsardakis, G. *J. Magn. Magn. Mater.* **2007**, *316*, e827–e830.
(33) Ghasemi, A.; Hossienpour, A.; Morisako, A.; Liu, X.; Ashrafizadeh, A. *Mater. Design* **2008**, *29*, 112–117.
(34) Wan, M.; Li, J. *J. Polym. Sci., Part A: Polym. Chem.* **1998**, *36*, 2799–2805.
(35) Singh, K.; Ohlan, A.; Kotnala, R. K.; Bakhshi, A. K.; Dhawan, S. K. *Mater. Chem. Phys.* **2008**, *112*, 651–658.
(36) Kazantseva, N. E.; Bespyatykh, Y. I.; Sapurina, I.; Stejskal, J.; Vilcakova, J.; Saha, P. *J. Magn. Magn. Mater.* **2006**, *301*, 155–165.
(37) Jacobo, S. E.; Aphesteguy, J. C.; Anton, R. L.; Schegoleva, N. N.; Kurlyandskaya, G. V. *Eur. Polym. J.* **2007**, *43*, 1333–1346.
(38) Qiu, J.; Shen, H.; Gu, M. *Powder Technol.* **2005**, *15*, 116–119.
(39) JCPDS Card No. 39−1433.
(40) Choi, J. W.; Han, M. G.; Kim, S. Y.; Oh, S. G.; Im, S. S. *Synth. Met.* **2004**, *141*, 293–299.
(41) Singh, K.; Ohlan, A.; Saini, P.; Dhawan, S. K. *Polym. Adv. Technol.* **2008**, *19*, 229–236.
(42) Colaneri, N. F.; Shacklette, L. W. *IEEE Trans. Instrum. Meas.* **1992**, *41*, 291–297.
(43) Singh, R.; Kumar, J.; Singh, R. K.; Rastogi, R. C.; Kumar, V. *New J. Phys.* **2007**, *9*, 40.

(44) Nicolson, A. M.; Ross, G. F. *IEEE Trans. Instrum. Meas.* **1970**, *19*, 377–382.
(45) Weir, W. B. *Proc. IEEE* **1974**, *62*, 33–36.
(46) Phang, S. W.; Hino, T.; Abdullah, M. H.; Karamoto, N. *Mater. Chem. Phys.* **2007**, *104*, 327–335.
(47) Smit, J.; Wijn, H. P. J. *Ferrites; Physical properties of ferrimagnetic oxides in relation to their technical applications*; Philips Technical Library: Eindhoven, Netherlands, 1959, p 244.
(48) Ishino, K; Narumiya, Y. *Ceram. Bull.* **1987**, *66*, 1469–1474.
(49) Dimitrov, D. A.; Wysin, G. M. *Phys. Rev. B* **1995**, *51*, 11947.
(50) Shilov, V. P.; Bacri, J. C.; Gazeau, F.; Gendron, F.; Perzynski, R.; Raikher, Y. L. *J. Appl. Phys.* **1999**, *85*, 6642.

AM900893D